L-mode-Edge Negative Triangularity Tokamak (NTT) Reactor

M. Kikuchi[1,2,3], T. Takizuka[4], S. Medvedev[5], T. Ando[6], D. Chen[7], J.X. Li[3], M. Austin[8], O. Sauter[9], L. Villard[9], A. Merle[9], M. Fontana[9], Y. Kishimoto[10], K. Imadera[10]

[1] National Institutes for Quantum and Radiological Science and Technology, Japan
[2]Institute of Laser Engineering, Osaka University, Japan
[3]Southwestern Institute of Physics, China
[4]Graduate School of Engineering, Osaka University, Japan
[5]Keldysh Institute of Applied Mathematics, RAS, Russia
[6]Ex-JAEA
[7]Key Laboratory of Neutronics and Radiation Safety, Institute of Nuclear Energy Safety Technology, Chinese Academy of Sciences, Hefei, Anhui, 230031, China
[8]Institute for Fusion Study, University of Texas, US
[9] Ecole Polytechnique Fédérale de Lausanne (EPFL), Swiss Plasma Center (SPC), CH-1015 Lausanne, Switzerland
[10]Institute of Advanced Energy, Kyoto University, Japan

Email: kikuchi.mitsuru@qst.go.jp

Abstract

The negative triangularity tokamak (NTT) is a unique reactor concept based on "power-handling-first" philosophy with the heat exhaust problem as the leading concern. The present paper exposes a reactor concept using L-mode edge based on negative triangularity tokamak (NTT) configuration, providing merits of no (or very weak) ELMs, larger particle flux and large major radius for power handling. It is shown that a reasonably compact (R_p from *9m* to *7m*) NTT reactor is possible by achieving higher confinement improvement (H_H=*1.5*) and/or by utilizing reasonably higher magnetic field (B_{max}=*15.5T*). Current physics basis and critical issues on its scientific and technical feasibility are discussed.

1. PHYSICS BACKGROUND OF NTT REACTOR

1.1. Power Handling Issues in H-mode

The tokamak is a promising confinement configuration having possible steady-state operation [1]. The current standard reactor confinement concept relies on D-shaped plasma with H-mode confinement having the edge transport barrier. However, the H-mode edge transport barrier produces critical power handling issues in transient ELM and in steady state SOL power e-folding length. The type-I ELM produces large amount of transient energy release to the divertor plates if the edge plasma

is in collisionless regime ($\nu^*<0.1$) associated with the excitation of the edge bootstrap current, for example $\Delta W_{ELM}\sim 21MJ$ in ITER [2]. Such large energy loss will damage the divertor plates: minimization of ELM energy loss is necessary for ITER and the complete elimination of ELM is required for the commercial use of fusion energy. The H-mode edge transport barrier also reduces particle flux across the separatrix to the neoclassical level; balancing with the parallel semi-sonic flow gives rise to the narrow heat flux width $\lambda_q \sim 1/B_p$ [3], [4]. Large reduction of the particle flux across the separatrix in the H-mode operation increases energy per particle to the divertor, and the formation of cold and dense, or the detached-divertor plasma becomes more challenging. For example, neoclassical particle outflux across the separatrix to a neoclassical level is an order of magnitude smaller than assumed value of fusion reactor to obtain cold and dense divertor condition [5]. The SOL density in the reactor should be high enough to form cold & dense divertor plasma. In high-density regime ($n_e>0.85n_G$), degradation of H-mode confinement has been observed due to the reduced temperature gradient. All these problems originate from the H-mode system and cast a question of the feasibility of H-mode as the reactor operation mode [6], [7].

1.2. Power Handling First

Historically, the priority of fusion research has been “plasma confinement first” and the discovery of H-mode naturally led it to become the standard operation mode. A survey of power handling challenges and an assessment of the negative triangularity-shaped tokamak (configuration, SOL flow, confinement, MHD stability and technical merits) as an alternative operation scenario of tokamak fusion reactor was made [5]. Negative triangularity tokamak “NTT” is a reactor concept based on “power-handling-first“ philosophy by locating long-leg divertor at outboard side with negative triangularity $\delta<0$ and making flux tube expansion to maximize heat exhaust surfaces. NTT configuration features a magnetic hill (i.e. specific volume $U=dV/d\Phi$ decreases with minor radius. Here V and Φ are volume and toroidal flux inside a flux surface, respectively. Simply speaking, the average toroidal field over the flux surface decreases with minor radius) and NTT has never been considered as a possible fusion reactor configuration during the long history of fusion research. Locating the X-point to the large major radius side ($R_x > R_p$), the wetted area of the divertor plates can

be larger leading to a geometrical reduction of the heat flux. If we use double-null (DN) divertor, this leads to up-down symmetric negative triangularity tokamak, DN-NTT [8], [9]. A single-Null (SN) NTT reactor was also designed and presented at the previous IAEA-FEC conference [10].

Locating the divertor at a larger major radius position maximizes the pumping conductance for an efficient particle exhaust especially from the inboard divertor [5]. In the standard D-shaped tokamak reactor design such as SSTR [11], the pumping conductance from inboard divertor side is an order of magnitude lower than that for outer divertor side. Since experiments showed large fuel deposition near the inboard divertor plate [12], strong pumping from the inboard divertor region is quite important. We can expect comparable exhaust conductance for both divertor pumping ducts for NTT reactor since both divertor legs locate at outboard side.

1.3. Plasma Confinement of NTT

Shaping the plasma to negative triangularity has favorable effect on energy confinement. The trapped electron mode (TEM) is one of important candidates of the turbulent transport in tokamaks as reviewed by Kadomtsev [13]. Experiments in ASDEX [14] and Tore-Supra [15] showed that the TEM plays an important role in turbulent transport in collisionless tokamaks. The TEM growth is enhanced by the precession drift resonance since the perturbed distribution function $g_e \sim 1/(\omega - \omega_{De})$, where ω_{De} is the trapped electron toroidal precession drift frequency. Drift de-resonance of the TEM is possible through number of ways, such as finite beta by Rosenbluth [16], Shafranov shift at high β_p operation by Connor [17], negative shear by Kadomtsev [18], elongation and negative triangularity by Rewoldt [19]. Among these mechanisms, the combination of negative shear, high β_p operation and the negative triangularity leads to an attractive operation scenario for the steady-state tokamak reactor. A comparative study of positive and negative triangularity tokamak plasmas in TCV during electron cyclotron (EC) heating [20], [21] (Figure 1) clearly demonstrated NTT can double the electron energy confinement time in the TEM-dominated regime without H-mode. TCV also compared the electron temperature fluctuation between NTT and standard D-shaped plasma (positive triangularity tokamak, PTT). Fontana [22] measured the turbulent electron temperature fluctuation $\delta T_e/T_e$ a using CECE (correlation electron cyclotron emission) in ohmically-heated low density plasmas. TCV's ohmically-

heated NTTs have better confinement than PTTs. They showed a clear reduction of both fluctuation amplitude and correlation length in NTT at normalized radius range $0.5<\rho_{vol}<0.8$ where $T_e>T_i$. GENE simulation for these discharges implies dominant mode is TEM [23] similar to the case of EC heating results in [21].

Another explanation of NTT improved confinement from the non-stiffness of the L-mode edge was made by Sauter [24]. He found that the core region ($r/a<0.8$) is stiff for heat transport above the critical temperature gradient but the edge region ($0.8<r/a<1.0$) is not stiff, suggesting different transport mechanisms dominate. He observed experimentally that L-mode edge in NTT has reduced transport, that may explain the TCV NTT improved confinement results [21]. Merlo [25] showed that the critical temperature gradient increases toward the edge and further increases in the negative triangularity consistent with Sauter's observation. Furthermore, Fontana's measurements of turbulent temperature fluctuation $\delta T_e/T_e$ as a function of R/L_{Te} in TCV [22] showed that the critical temperature gradient $(R/L_{Te})_{crit}$ in NTT is larger than that in PTT consistent with Merlo's predictions. Resistive ballooning mode (RBM) is a possible candidate of edge and SOL turbulent transport. The RBM is localized along the field line in the bad curvature region. Riva [26] analyzed the linear and nonlinear RBMs showing that the RBMs in the vertically elongated DN-NTT are more stable. The physical explanation of the stabilizing mechanism is that the magnetic field line pitch is large near the outer mid-plane and the particle residence time in bad curvature region is shorter. This mechanism may be commonly applicable for all types of ballooning-like instabilities in DN-NTT.

Recently, DIII-D [27], [28], [29] made a groundbreaking experiment demonstrating $H_H=1.2$ and $\beta_N=2.6$ simultaneously with L-mode-like edge in NTT showing that the proposed NTT reactor condition ($H_H=1.12$, $\beta_N=2.1$) [10] can be exceeded. DIII-D has flexible shaping capability to produce up-down symmetric inner-wall limited near-DN NTT configuration (see Figure 1). While inner-wall limited auxiliary heated D-shaped plasma went to the limiter H-mode (Z_{eff} (0) went up to 3.5-4 after L-H transition from 2.0-2.5 in L-mode phase), NTT stayed at L-mode (Z_{eff}(0) stays at 2.0-2.5) with improved confinement to achieve $H_H=1.2$ at $\beta_N=2.6$. Impurity contamination is lower and the neutron emission was doubled in NTT as reported by Austin [29]. These DIII-D NTT plasmas are relatively

high density ($n_e(0)$~$6x10^{19}m^{-3}$) but still in the mixed ITG/TEM regime dominated by TEM as shown by Marinoni [30].

1.4. L-mode Edge Operation

Current tokamak reactor designs are based on the H-mode operation. Considering the power-handling issues given above, the L-mode edge is preferred as a robust operation mode in fusion reactor. L-mode also provides much larger particle flux than H-mode necessary to form cold & dense divertor (i.e. neoclassical particle flux in H-mode is too small [5]). DIII-D experiments [29] showed that inner-wall limited NTT edge stayed in L-mode even at large NB heating power (P_{NB}=*11MW*), while inner-wall-limited D-shaped plasma went to the limiter H-mode for a same heating power. The SOL density in DIII-D NTT L-mode edge is much higher than that of H-mode. Since the key impurity control mechanism in the fusion reactor is the parallel friction force to compete with the thermal force to prevent impurity back flow, sustainment of high SOL density is key to the impurity control.

While L-mode edge turbulent transport may be weaker in NTT than that of L-mode edge PTT [26], it will provide a better solution for the reactor power and particle exhaust than those by the H-mode operation of PTT. Research toward the sustainment of L-mode edge with improved confinement at reactor-relevant normalized beta is desired in large higher field negative triangularity tokamaks as well as the establishment of L-H power threshold scaling on negative triangularity.

While all these experimental and theoretical results are encouraging for the proposed NTT reactor with L-mode edge, TCV and DIII-D experiments are of inner-wall limited plasmas. Respective roles of inner-wall limiter and X-point operation are important missing pieces of information. For the latter subject, it reminds us that the original JT-60 had divertor X-point in the outboard mid-plane and showed very short period of H-mode but returned to L-mode confinement [31]. Possible sustainment of L-mode edge in a reactor is further discussed in section 3.2.

1.5. MHD Stability of NTT

The MHD stability of NTT has been studied in our previous papers by Medvedev [9], [10]. Since NTT magnetic configuration features magnetic hill, the localized Mercier mode stabilization is only possible with finite magnetic shear, i.e. *1/4*>D_M, where *1/4* comes from shear stabilization of the localized mode and D_M is the Mercier index, where $D_M > 0$ corresponds to the magnetic hill

($D_M=8\pi r(dp/dr)(1-q^2)/s^2B^2$ in circular plasma). Ohkawa's comet shape ($\kappa<1$ and $\delta<0$) [32] is the exception of negative triangularity with magnetic well, where a single X-point is located in the inboard side. Mercier stability is significantly modified including the kinetic effects such as thermal trapped ion effect given by Kruskal-Oberman [33] and fast ion effect, especially in the central region, where the stability condition is given by $1/4>D_{MM}=D_M+D_{KO}+D_h$, $D_{KO}\sim-0.47(8\pi p_i/s^2B^2)/(r/R)^{0.5}$ is the Kruskal-Oberman correction and $D_h \sim q^2(2Rr)^{0.5}dp_h/dr/s^2B^2$ is the energetic ion correction as discussed by Porcelli [34].

Medvedev [9] studied and optimized the ideal MHD stability of a κ_x=1.5 DN-NTT. The DN-NTT is characterized by the high magnetic shear near the separatrix. Stable high-normalized beta equilibrium is obtained by setting $dp/d\psi$ close to Mercier stability limit in the inner half region ($/\psi/^{1/2}<0.5$) as well at the very edge considering the high edge magnetic shear. To take the kinetic stabilization mentioned above into account, the case of higher pressure-gradient in the inner half region could be considered. Ballooning mode sets $dp/d\psi$ profile in the outer half region (($/\psi/^{1/2}>0.5$)). Using this basic idea, stability limit to ideal MHD modes was studied. The beta limit of NTT strongly depends on l_i (internal inductance). For $A=2.6$ ($R_p=7m$, $a_p=2.7m$, $\kappa=1.5$, $\delta=-0.9$), $I_N=I_p/a_pB_t=0.9$ and $l_i=0.9$ (positive shear; PS), the beta limit is $\beta_N=3.2$ without wall stabilization and $\beta_N=3.3$ with wall stabilization ($a_w/a_p=1.3$) [9]. If we reduce $l_i=0.75$, the beta limit is reduced to $\beta_N=2.4$ without wall stabilization and $\beta_N=2.6$ with wall stabilization. While ballooning mode is stable for negative shear (NS) region, NS configuration has relatively low beta limit $\beta_N=2.1$ without wall stabilization. This is marked difference with PTT NS plasma. The DN-NTT is more prone to the axisymmetric instability. Relatively close fitting *6cm* steel stabilizing shell at $a_w/a_p=1.25$ is needed to reduce the growth rate of $n=0$ axisymmetric mode $\gamma_{n=0}=95s^{-1}$, which requires good feedback control of axisymmetric mode [9].

More elongated NTT can be stable to the axisymmetric modes ($n=0$) for the single-null divertor (SN-NTT). Medvedev studied the stability of SN-NTT for $A=3$ ($R_p=9m$, $a_p=3m$, $\kappa=1.8$, $\delta_u=-0.4$ *and* -0.07, $\delta_l=-0.9$), $I_N=1.19$ ($I_p=21MA$, $B_t=5.86T$) [10]. For an upper triangularity $\delta_u=-0.4$ *and* $l_i=0.84$, the beta limit is $\beta_N=2.79$ without wall stabilization and $\beta_N=3.3$ with wall stabilization ($a_w/a_p=1.3$) while edge magnetic shear is smaller than that of DN-NTT. For this configuration, the growth rate of the

axisymmetric mode with a_w/a_p=1.3 is $\gamma_{n=0}=14s^{-1}$ for *6cm* steel stabilizing shell. For an upper triangularity $\delta_u=-0.07$ and $l_i=0.84$, the beta limit is $\beta_N=3.14$ without wall stabilization and $\beta_N=3.56$ with wall stabilization ($a_w/a_p=1.3$). The growth rate of the axisymmetric mode with a_w/a_p=1.3 is $\gamma_{n=0}=11s^{-1}$ for *6cm* steel stabilizing shell for this configuration.

We studied the contribution of edge pedestal in optimized pressure profile in NTT. Figure 2 a) shows optimized pressure profile in NTT. Pressure should have near-flat profile in the central region. Figure 2 b) shows the radial profile of $p'=dp/d\psi$ for a typical A=3, κ=1.8 SN-NTT equilibrium optimized for ideal MHD stability. The inner half is shaped to have Mercier-limiting profile, the outer half is ballooning-limiting profile and the very edge is designed to have Mercier-limiting profile. To demonstrate non-negligible pedestal contribution to the beta limit, we set dp/dψ smoothly go to zero in the pedestal region. We found 5% reduction in normalized beta.

Reduction of the pedestal beta limit is one of the important targets of the NTT reactor design to minimize energy loss during the ELM event. Merle [35] made EPED-CH calculations and showed that the pedestal pressure for the NTT is 4 times less than PTT even if it goes to H-mode, a similar reduction can be expected for ELM energy losses since these two quantities are often correlated. Merle identified that the key parameter is the average triangularity $\delta=(\delta_l+\delta_u)/2$. Figure 3 shows the normalized pedestal pressure calculated by EPED-CH as a function of the average triangularity δ. Typically $P_{ped}=9.2$ *kPa* (0.1% of magnetic pressure) will be a limiting pedestal pressure in NTT reactor much smaller than the typical positive triangularity tokamak value of $P_{ped}=39$ *kPa* (0.4% of magnetic pressure). Thus, the edge bootstrap current to excite surface kink modes is expected to be small. While NTT has lower pedestal pressure and lower ELM energy loss if it happens, reactor operation will need complete suppression of ELM [36]. Enhanced pedestal radiation and SOL radiation to sustain L-mode edge without ELM will be a key. Also a detached or semi-detached divertor has to be carefully controlled. Lower pedestal pressure limit will certainly help to minimize the damage of plasma facing components in case of off-normal events.

2. TECHNICAL DESIGN OF NTT REACTOR

2.1 Configuration Designs

The NTT configuration design was started using the inverted D-shaped TFC for the DN-NTT [9]. Figure 4 shows revised PFC designs for DN-NTT with reduced elongation (κ_x=1.5) to meet the vertical stability of DN-NTT. This configuration can be realized by a reasonable set of equilibrium coils $\Sigma I_{PF}/I_p=6.7$ due to closer equilibrium coils. However, mechanical support for the centering and bending forces of TF coils are expected to be quite challenging.

Considering the above difficulty, we decided to use racetrack shape TF coils, where we can adopt standard wedge support for the centering force. We also decided to move all internal PC coils outside of the TFC for easier manufacturing. We adopted radial disk structure used in ITER and SSTR [11] to ensure radial force transmission. With all these changes, equilibrium shaping-coils are more distant from the NT-shaped plasma. Considering the better positional stability, reasonable normalized beta limit and the up-down power sharing issue in DN, we adopted the SN configuration for the NTT with modest confinement improvement factor $H_H=1.12$. The maximum field is limited to $B_{max}=13.6T$ due to stress limit *800MP* and the aspect ratio $A=R_p/a_p=3$. This gives rise to a large reactor size and current, i.e. $I_p=21MA$, $R_p=9m$, $B_t=5.86T$, $E_{TFC}=170GJ$ with the TF coil dimension of 15m width and 20m height. Major coil parameters of Figure 5 a) are shown in Table 1. Number of TF coils is *18*. Total Ampere Turns is *263MAT* with a conductor current of *126kA*. Number of turns/coil is *116* and the winding structure is double pancake using *6* radial disks. The discharge constant of TF coil is *12* second corresponding to the terminal voltage of *12.5kV* for quench protection assuming quench detection is within *2* second. TF conductor is designed using the standard ITER-like *Nb3Sn* superconductors design criteria as given in the next subsection. The set of poloidal field (PF) coils enables the shaping of upper plasma in order to vary its triangularity, δ_u= *-0.4 (orange) to* δ_u= *-0.07 (blue),* with vertical elongation $\kappa_x=1.8$ at the separatrix and $q_{95}=3.0$ and $q_{95}=3.1$, respectively. We obtain these shaping variations with $\Sigma I_{PF}/I_p=6.8$ and $\Sigma I_{PF}/I_p=5.9$, respectively. These values are comparable to that of DN-NTT with inverted-shaped TF coil.

To construct a more compact fusion reactor, we made a parameter survey through the major radius (R_p=*9-7m*) scan for A=3 and A=*3.5* (Figure 6) while keeping the confinement measure, $H_H I_p A$=*69.3MA*, and the engineering safety factor, q_{eng}=*3.5*. We also kept the normalized density n/n_{GW}=*0.85*. Procedures in this parameter scans are introduced in the appendix A.

We increased κ_x=*1.8* to κ_x=*2.0* for the A=*3* scan while n=*0* growth rate becomes $\gamma_{n=0}$=*40s*$^{-1}$. This could be managed by the active feedback control. We assumed κ_x=*1.85* for the A=*3.5* scan. In the parameter scan, H_H is fixed in solid line H_H=*1.2* and H_H is increased *from 1.1 to 1.5* as R_p is reduced from *9m* to *7m* in broken line.

Parameter surveys for the A=*3* case are shown in Figure 6 a) and b). Solid lines of Figure 6 a) and b) show that reduction of major radius to R_p=*7m* is possible while plasma current I_p and β_N are almost kept constant but it requires higher magnetic field B_t~*16T* to keep q_{eng}=*3.5*. Moreover, the fusion power P_f and the average neutron flux q_n also increase. Broken lines of Figure 6 a) and b) show that reduction of major radius to R_p=*7m* is also possible with improved confinement (H_H=*1.5)* while B_{max} is nearly constant. In this case, the fusion power is reduced to P_f=*2GW* and the neutron wall load stays almost constant q_n~*1.4-1.5MW/m*^{2} while the normalized beta β_N becomes higher than the case for R_p=*9m* (β_N=*2.1)*. Based on this parameter scan, we finalized the parameter set of the steady-state operation point using the system code shown in subsection 2.3 as I_p=*15.4MA*, B_t=*5.94T*, H_H=*1.5,* n=*0.77 x 10*^{20} *m*$^{-3}$, P_f=*2.07GW,* B_{max}=*13.5T*, β_N=*2.7*, P_{CD}=*106MW, Q=19.5*. Configuration design for highly shaped NTT with upper triangularity δ_u=*-0.4* and lower triangularity δ_l=*-0.9* is realized by a set of shaping coils with $\Sigma I_{PF}/I_p$=*8.1*. The coil configuration is shown in Figure 5 b). Since B_{max}=*13.5T*, standard wedge support allows maximum stress within *800MPa* with the TF coil dimension of *12m* width and *16m* height. TF magnetic energy is reduced to *86.5GJ* with the total Ampere Turns of *207MAT* with the conductor current *100kA*. Number of turns/coil is 116 and the winding structure is double pancake using *6* radial disks. The discharge constant and the terminal voltage are 10second and 10kV, respectively.

Parameter surveys for the A=*3.5* case (κ_x=*1.85*) are shown in Figure 6 c) and d). Solid lines of Figure 6 c) and d) show that reduction of major radius to R_p=*7m* is also possible while plasma current

I_p and β_N are almost kept constant but it requires higher magnetic field B_t~*19.5T* for fixed H_H=*1.2* to keep q_{eng}=*3.5*. The plasma volume is smaller (V_p~*1000m*^{3}) compared with the *A=3* case (V_p~*1500m*^{3}). Broken lines of Figure 5 c) and d) are parameter survey for *A=3.5* case with varying H_H factor and show that reduction of major radius to R_p=*7m* is also possible with improved confinement (H_H=*1.5*). Final parameter set of the steady-state operation is determined by the system code as, I_p=*13.2MA*, B_t=*7.53T*, *n=0.9 x 10*^{20} *m*$^{-3}$, P_f=*1.9GW,* B_{max}=*15.5T*, β_N=*2.5*, P_{CD}=*115MW*, *Q=21.2*. Similar shaping with upper triangularity δ_u=*-0.4* and lower triangularity δ_l=*-0.9* is realized by a set of shaping coils with $\Sigma I_{PF}/I_p$=*8.25*. The coil configuration is shown in Figure 5 c). Since B_{max}=*15.5T*, wedge support region is extended toward the machine center to keep maximum stress below 800MPa. The TF coil dimension is *11m* width and *14m* height. TF magnetic energy is *104GJ* with total Ampere turn of *263MAT* with the conductor current *100kA*. Number of turns/coil is *146* and the winding structure is double pancake using *7* radial disks. The discharge constant and the terminal voltage are *12* second and *10kV*, respectively. TF conductor is designed using the standard ITER-like $N_{b3}S_n$ superconductors design criteria and also more advanced *Bi2212* high T_c superconductor as given in the subsection 2.2.

For all three TF magnet designs, we selected discharge constant to keep the quench temperature rise of *150K*.

2.2 Conductor design of TF coils

For the three reactor configurations above, we developed two conductor designs for each TF coil. We assumed high J_c *(1000A/mm*^{2}*) Nb3Sn* strand for the design extrapolated from recent development of high J_c strand for ITER [37]. Design parameters of these six conductors are shown in Table 2 and their conductor shapes are shown in Figure 7. Our design utilized $J_c(B,T,\varepsilon)$ parameterzation by Bottura [38] for *Nb3Sn* and the paper from Rey [39] for *Bi2212*.

In the *A=3,* R_p=*9m* designs with B_{max}=*13.6T* (Figure 5 a)), we can use *Nb3Sn* cable-in-conduit (*CIC*) conductor with *SS* conduit or T_i conduit at *5.0K* operating temperature. The TF conductor of ITER uses *SS* conduit but the thermal expansion coefficient of SS is different from that of *Nb3Sn* strand and has to assume a large strain. The *Nb3Sn CIC* conductor with *SS* conduit is designed to

allow higher total operating strain (*-0.6%*). The ratio of SC and Cu strands is *2 : 1* with a void fraction of *33.3%*.

Titanium (T_i) has a thermal expansion coefficient close to *Nb3Sn* superconductor and is effective to reduce strain of the SC. Ando [40] proposed to use T_i as a jacket of superconductor and T_i -jacket conductor has been manufactured as the ITER TF insert conductor [41] and the effectiveness of T_i jacket is demonstrated [42]. The design strain can be reduced from *-0.6%* in SS jacket to *-0.05%* in T_i jacket. Reduction of design strain leads to a significant increase in operating critical current density. Therefore, we can increase *Cu*/ non-*Cu* ratio from *1.0* to *2.0* (or reduce amount of *Nb3Sn* in the strand). Ratio of SC and Cu strands is also changed from *2 : 1* to *5 : 4* as seen Figure 7. The cable diameter is reduced from *66mm* to *61.8mm*. The conductor has central cooling channel with the outer diameter *OD=11mm* and the inner diameter *ID=9mm* for the supercritical Helium forced flow cooling.

In the *A=3*, R_p*=7m* configuration, conductor design is similarly made for *SS* conduit and T_i conduit. For a *SS* conduit design, total operating strain is *-0.6%* and the Cu/Non Cu ratio is *1.0* and the ratio of SC and Cu strands is *2 : 1* with a void fraction of *33.3%*. For a T_i conduit design, total operating strain is *-0.05%* and the Cu/Non Cu ratio is *2.0* and the ratio of SC and Cu strands is *1 : 2* with a void fraction of *33.3%*. Helium coolant channel design is same for *A=3,* R_p*=9m* configuration.

In the *A=3.5,* R_p*=7m* configuration with B_{max}*=15.5 T*, we can also use *Nb3Sn* cable-in-conduit (*CIC*) conductor at *5.0K* operating temperature if we use T_i conduit. The *SS* conduit adopted for ITER will have difficulty by a large reduction of J_c due to the large strain due to the difference in thermal expansion coefficient between *SS* and *Nb3Sn*. High T_c superconductor is attractive technology for the magnetic confinement fusion providing compact reactor configuration such as *VECTOR* [43] where the high T_c conductor designs are successfully developed [44], [45]. As long as *Nb3Sn* design is possible, it is more reliable and economical at present to use *Nb3Sn* design. However, recent development of high T_c superconductor is quite remarkable and the critical current density of *Bi2212* at *15T* exceeded that of *Nb3Sn* as reported by J. Jiang [46]. This makes it reasonable to give a design option using the *Bi2212* at an operating temperature of 20K under moderately high magnetic field (*15.5T*). At this elevated temperature, the heat capacity of *PbSn* alloy is quite large and *Bi2212* strands are impregnated in *PbSn* alloy and its conductor size is comparable with *Nb3Sn* as shown in Figure 7.

The maximum allowable stress of cryogenic steel will be reduced by *7%* at *20K* but an addition of backing cylinder between CS coil gap will satisfy the stress requirement.

2.3 System code assessment of steady-state operation in NTT Reactor

The current tokamak system code is based on the shaped cross section equilibrium database. However, the negative triangularity equilibrium database is not included and the code was not applicable for NTT. Sauter expanded the equilibrium database to include NTT [47] and the resultant formula is included in the system code by Chen [48]. Results of the system code for three configurations in Figure 5 are summarized in Table 3. First parameter set from left corresponding to Fig. 5 a) is the single-null negative triangularity tokamak (SN-NTT) reactor proposed in the last Fusion Energy Conference (2016) [10]. This reactor has fusion power P_F~*3GW* and the transport power across the separatrix is P_{trans}~*594MW*. It operates at relatively lower density $n_e=6.3 \times 10^{19} m^{-3}$ for the steady-state operation with the current drive power of $P_{CD}=168MW$.

Newly proposed reactor parameters are shown in 2nd and 3rd set of parameters in Table 3. We found that Q~20 steady state operation may be possible even at reduced size machines if high confinement ($H_H=1.5$) is achievable for $A=3$ case and also if both high field ($B_{max}=15.5T$) and high confinement ($H_H=1.5$) are achievable for $A=3.5$ case. Operating normalized beta in $A=3$ and $A=3.5$ are within no-wall limits. Here $\beta_N^{NW}=2.89$ $(A=3)$ and $\beta_N^{NW}=2.87$ $(A=3.5)$. Transport powers across the separatrix are *384MW (A=3)* and *338MW (A=3.5)*, respectively. The power required for steady-state operation is *96.6MW* for $A=3$ design and *101MW* for $A=3.5$ design, respectively.

2.4 Divertor and FTE (Flux Tube Expansion)

Locating the divertor hit-point on the large major radius side provides the opportunity of a larger wetted area. Long-leg divertor also contributes to reduce the divertor heat flux through radiation between X-point to hit-point. However, magnetic pitch angle increases rapidly away from the X-point and the width of the flux tube becomes narrower. The “Flux-Tube-Expansion divertor” concept [49] is adopted to reduce magnetic pitch near the divertor plate. An important merit of NTT is that FTE can be applied in both inner and outer divertor legs. Herrmann [50] gave a minimum field line angle of 1^o, which is limited by the divertor alignment in the toroidal direction. Figure 8 show typical NTT equilibria without and with FTE ($I_{FTE}=2.5MA$). Without FTE, the angles between the

magnetic field line and the divertor plate surface at outer and inner divertor plates are $\alpha=8.7^o$ and $\alpha=5.1^o$, respectively. Application of FTE ($I_{FTE}=2.5MA$) reduces these angles to $\alpha=2.1^o$ for outer divertor plate and $\alpha=2.6^o$ for inner divertor plate, respectively. Dramatic reduction of field line angle is possible especially for the outer divertor.

Figure 9 shows the divertor geometries with FTE-coils of $I_p=15MA$, $R_p=7m$ NTT configuration. Separatrix line is shown in red (color online). A 1 mm SOL flux tube width at the outboard mid-plane are projected to a 3.7mm width flux tube in the inboard mid-plane, a 4.3mm width flux tube in the inboard plate, and 4.8mm width flux tube in the outboard divertor plates (black lines). If the divertor plates are more inclined (green lines), grazing angles are close to 1 degree and the length along the plates can be 10mm as shown in Figure 9. Assuming the SOL heat flux width of NTT L-mode edge is twice of that of PTT H-mode, the heat flux width at the divertor plates could be *20mm*, each. We may expect wider heat flux width near the detached condition as well [51].

3. DISCUSSIONS

The scientific feasibility of operating NTT as a reactor is still much less well established than for a PTT due to lack of experimental and theoretical investigations. Here we address some key questions and provide implications to future scientific research.

3.1 Feasibility of Improved Confinement in DEMO Reactor Regime

Many of proposed DEMOs such as EU-DEMO ($R_p=9m$, $P_{fus}=2GW$) operated in high-density regime ($n_e>10^{20}m^{-3}$) may be in the ITG dominant regime. A key question is if the proposed NTT reactors can have improved confinement with L-mode edge. The proposed steady-state operations of NTT reactor will be at lower densities ($n_e=0.6\text{-}0.9 \times 10^{20}m^{-3}$ in Table 3) due to a limitation of non-inductive current drive efficiency. We still do not know if the reactor can have required improved confinement in these density regimes while recent experiments in TCV and DIII-D are encouraging (especially high density DIII-D operation is in the TEM-dominant regime). Further progress of experimental and theoretical efforts as well as turbulent transport modeling efforts for the NTT reactor may provide better physics basis for the NTT reactor.

Considering the recent experimental and theoretical progress, local linear TEM stability may be not the sole reason for the actual confinement improvement observed in TCV and DIII-D. Improved confinement may be also enhanced by the better stability against the RBM in the non-stiff region ($0.8 < r/a < 1$) in the L-mode within the lowered pedestal pressure limit. Near the magnetic axis, both NTT and PTT have almost zero triangularity but still have improved confinement in both TCV and DIII-D. This may be a non-local effect [52], the size scaling of which is presently unknown. Further global nonlinear gyrokinetic simulations are needed in order to determine whether the effect survives in a reactor-size NTT. Also reduced temperature fluctuation in NTT relative to PTT is observed even in $T_e/T_i \sim 1$ ITG/TEM mixed regime with a collisionality range $0.3 < 1/\nu_{eff} < 1$ in recent TCV experiments [23]. DIII-D high beta results at $n_e(0) \sim 6.0 \times 10^{19} m^{-3}$ [30] also implies that improved confinement can exist even under the ITG/TEM mixed regime.

3.2 Avoiding L-H Transition in Reactor Regime

One of the key proposals in this paper is to stay in the L-mode edge in the NTT reactor. According to the ITER physics basis [53], P_{LH} (MW) scales as $P_{LH}=0.042\, n_{20}^{0.73} B_t^{0.74} S^{0.98}$. Here n_{20}, B_t and S are electron density (10^{20}m^{-3}), toroidal field (T), and surface area (m^2), respectively. Values of P_{heat}/P_{LH} in DIII-D NTT and PTT are both ~6.7 and NTT stays in L-mode edge and PTT made L-H transition. The values of P_{transp}/P_{LH} for three reactors in Table 3 are *3.5 ($A=3$, $R_p=9m$)*, *2.2 ($A=3$, $R_p=7m$)*, and *2.6 ($A=3.5$, $R_p=7m$)*, respectively. Considering the DIII-D NTT stays at L-mode edge even at 6.7 times L-H transition power scaling, there might be a possible way to keep NTT reactor edge staying in L-mode edge.

Inner-wall contact may have an important role in suppressing the L-H transition but the contact area in DIII-D NTT is much smaller than PTT limiter H-mode. The absence of X-point is another critical issue left for future study, while the existence of limiter H-modes in various tokamaks JFT-2M [54], JT-60 [55], JIPP T-IIU [56], TCV [57] implies X-point is not essential for the L- to H-mode transition. The role of negative triangularity on the L- to H-mode transition is a crucially important experimental and theoretical subject for future research. If the power threshold for L- to H-mode transition in NTT in divertor configuration is lower than transport power in Table 3, enhanced core

and edge radiation may be needed to supress L- to H-mode transition to stay at L-mode edge. Note that designing NTT SN magnetic field towards unfavorable direction should further ensure an L-mode state.

3.3 Possible power handling scenario in NTT reactors

Fusion reactor needs to operate stably and reliably for year-long operation. Current database for long pulse operation is still very limited even for PT tokamak as well as stellarators as shown in Figure 10 [57], [58]. Considering the heat flux level of existing power system such as fission power plants (q_{max}~$1MW/m^2$) and fossil power plants (q_{max}~$0.3MW/m^2$), the maximum heat flux of magnetic fusion power plant may need to be reduced to a few MW/m^2.

For example, case for $A=3$, $R_p=9m$ configuration, the total heating power is $P_{total}=761MW$, of which $167MW$ (22%) are radiated in the core-region. Further 20% $(150MW)$ could be radiated in the L-mode edge region, which could be free from confinement degradation. High SOL density in the L-mode edge would help to further radiate in the SOL region and also long-leg (X-point to divertor plate : $2.6m$) divertor, which could radiate ~50% of total heating power [58]. Remaining 8% (~$60MW$) would be handled by two divertor plates with total effective wetted area of $S_{plate}=30m^2$ to handle radiation, conduction and convection heat flux to stay at a few MW/m^2 heat flux. Since toroidal length at the divertor hit points are $70m$ for inboard divertor plate and $88m$ for outboard divertor plate, effective poloidal length of the divertor power handling area (D-PHA) of $0.2m$ for each plate would be sufficient. Precise control of power inlet to the D-PHA is a critical R&D issue.

In the European DEMO scenario [51], higher core radiation fraction is envisaged but is limited to assure L- to H-mode transition by the condition $P_{sep}>1.3P_{LH}$. On the other hand, the NTT reactor may offer possible high core radiation scenario to stay at L-mode edge and to reduce divertor heat load.

4. SUMMARY

Current power handling challenge in tokamak D-shaped H-mode is quite serious and world fusion research effort is devoted to resolve this problem with some success. However, we still do not know if we can open the way of power handling for year-long operation in this route. The Negative Triangularity Tokamak (NTT) reactor concept is proposed as an alternative route for tokamak power

handling. NTT now has good experimental and technical basis while there are still many physics issues to be clarified in the experiment and simulation.

5. ACKNOWLEDGEMENT

The authors appreciate TCV experimental and DIII-D experimental teams as well as their theory and simulation teams to clarify key physics issues related to NTT configuration. The authors also appreciate valuable constructive comments by the referees. This work was supported in part by the Swiss Naitonal Science foundation and carried out in part within the framework of the EUROfusion Consortium and has received funding from the Euratom research and training programme 2014 - 2018 and 2019 - 2020 under grant agreement No 633053. The views and opinions expressed herein do not necessarily reflect those of the European Commission.

APPENDIX A

We briefly describe equations used for the parameter scan in subsection 2.1. While there is some possibility that NTT confinement scales differently, we kept $H_H I_p A$ constant during the parameter scan ($H_H I_p A$ = 69.3MA in the present study) since it is a good measure of fusion performance as discussed in ITER physics basis [59]. Here H_H is confinement enhancement factor over the IPB98(y,2) scaling [60], I_p is plasma current and $A = R_p/a_p$ is aspect ratio.

A relation between I_p and B_t (toroidal magnetic field at the plasma major radius R_p) is given by a certain value of engineering safety factor $q_{eng} = \pi(1+\kappa^2)a_p^2 B_t/\mu_0 R_p I_p$ (q_{eng}=3.5 in the present study). The elongation κ is tentatively chosen as $\kappa = 2.0$ at $A = 3$ and $\kappa = 1.85$ at $A = 3.5$ (see Table 1). The maximum toroidal field is determined as $B_{max}R_c = B_t R_p$, where R_c is the inner major radius of a TF coil giving the maximum field. We put a distance between TF coil and plasma, $\Delta_c = R_p - a_p - R_c$, to install the vacuum vessel and blanket (Δ_c = 1.6m for simplicity in the present study).

Thus we can make a parameter scan by varying R_p, and obtain results of Figs. 6 (a) and (c), i.e., I_p, B_t and B_{max} for given A and H_H. The H_H value is set constant, H_H = 1.2, for solid lines in Fig. 6, while it is varied for broken lines as H_H = 1.1 at R_p = 9m and H_H = 1.5 at R_p = 7m with a linear relation $H_H = 1.1 + 0.2(9 - R_p[\mathrm{m}])$.

Next we set the operation electron density n_e so that the Greenwald-density fraction, $f_{GW} = n_e/n_{GW}$ is constant (f_{GW} = 0.85 tentatively in the present study), where $n_{GW}[10^{20}\mathrm{m}^{-3}] = I_p/\pi a_p^2$ [MA/m^2]. It is a future work to find an optimum f_{GW} value for the reactor performance. It is noted that the burning-plasma temperature T is determined mainly by $H_H I_p A$ value ($T \approx$ 17keV at $H_H I_p A \approx$ 70MA; see Table 1). Then the normalized beta, $\beta_N = (100 a_p B_t/I_p)\ (4\mu_0 n_e T/B_t^2)$, is considered proportional to $a_p n_e/B_t I_p \sim f_{GW}/a_p B_t$ under the constant $H_H I_p A$ condition. Similarly the fusion power P_f is given in proportion to $n_e^2 V_p \sim f_{GW}^2 I_p^2 R_p/a_p^2$, where $V_p = 2\pi^2 \kappa R_p a_p^2$ is plasma volume (a reference value, P_f = 3GW at A = 3, R_p = 9m and H_H = 1.1, is applied in the present study; see Table 1). The neutron wall load is evaluated as $q_n = 4P_f/5S_w$, where the wall surface area is simply calculated as $S_w = 2\pi^2(1+\kappa)R_p(a_p + \Delta_p)$ with a gap Δ_p between plasma and wall (Δ_p = 0.3m in the present study). We obtain results of Figs. 6 (b) and (d), i.e., β_N, P_F and q_n for given A and H_H.

REFERENCES

[1] M. Kikuchi, M. Azumi, Steady State Tokamak Research – Core Physics, Rev. Mod. Phys. **84**, 1807(2012)

[2] A. Loarte, G. Saibene, R. Sartori, D. Campbell, et al., Characteristics of type I ELM energy and particle losses in existing devices and their extrapolation to ITER, Plasma Phys. Control, Fusion **45**, 1549(2003)

[3] R.J. Goldston, Heuristic drift-based model of the power scrape-off width in low-gas-puff H-mode tokamaks, Nucl. Fusion **52**, 013009(2012)

[4] T. Eich, B. Sieglin, A. Scarabosio, W. fundamenski, R.J. Goldston, A. Herrmann, and ASDEX Upgrade Team, Inter-ELM Power Decay Length for JET and ASDEX Upgrade: Measurement and Comparison with Heuristic Drift-Based Model, Phys. Rev. Lett. , 107, 215001(2011)

[5] M. Kikuchi, A. Fasoli, T. Takizuka, P. Diamond, S. Yu Medvedev, et al., Negative Triangularity Tokamak as Fusion Energy System, 1st International E-Conference on Energies March 14, 2014, E002, DOI:10.3390/ECE-1-E002, http://www.sciforum.net/conference/ece-1/paper/2321

[6] M. Kikuchi, T. Takizuka, Is H-mode relevant for Fusion Reactor, Plenary talk at US-EU TTF 2013 (Santa Rosa, USA, 2013), http://ttf2013.ucsd.edu/TTF_Meeting/Presentations.html

[7] M. Kikuchi, T. Takizuka, M. Furukawa, Negative Triangularity as a Possible Tokamak Scenario, Proc. 12th Asia Pacific Physics Conference (July 14-19, 2013, Makuhari), JPS Conf. Proc. 1 (2014)015014

[8] M. Kikuchi, S. Yu Medvedev, T. Takizuka, A. Fasoli, Y. Wu, et al., Perspective of Negative Triangularity Tokamak as Fusion Energy System", 42th EPS Conf. on Plasma Physics and Controlled Fusion, volume ECA vol 3 (Lisbon, Portugal) P4.179 (http://ocs.ciemat.es/EPS2015PAP/pdf/P4.179.pdf)

[9] S. Yu Medvedev, M. Kikuchi, L. Villard, T. Takizuka, P. Diamond, et al., The negative triangularity tokamak: stability limits and prospects as a fusion energy system, Nucl. Fusion **55**, 063013 (2015)

[10] S. Yu Medvedev, M. Kikuchi, T. Takizuka, et al., Single Null Divertor in Negative Triangularity Tokamak, 26th IAEA Fusion Energy Conference, 17-22 October 2016, Kyoto, Japan. https://nucleus.iaea.org/sites/fusionportal/Shared%20Documents/FEC%202016/FEC2016_ConfMat_Online.pdf , paper EX/P3-47 ; See also M. Kikuchi, S. Medvedev, D. Chen, et al., Single null negative triangularity tokamak reactor concept,18th International Congress on Plasma Physics (ICPP2016), June 27-July1, Kaohsiung, Taiwan, paper A4A1-1 http://capst.ncku.edu.tw/ISAPS/ICPP2016/Book%20of%20Abctracts.pdf

[11] M. Kikuchi, R.W. Conn, F. Najmabadi, Y. Seki, Recent directions in plasma physics and its impact on tokamak magnetic fusion design, Fusion Eng. Design **16**, 253 (1991)

[12] G. Federici, C.H. Skinner, et al., Plasma-Material Interactions in current tokamaks and their implications for next step fusion reactors, Nucl. Fusion **41**, 1967 (2003)

[13] B.B. Kadomtsev, O.P. Pogutse, Trapped particles in toroidal magnetic systems, Nucl. Fusion **11**, 67(1971)

[14] F. Ryter, C. Angioni, A.G. Peeters, F. Leuterer, W. Suttrop, and ASDEX Upgrade Team, Experimental Study of Trapped-Electron-Mode Properties in Tokamaks: Threshold and Stabilization by Collisions, Phys. Rev. Lett. **95**, 085001(2005)

[15] W.L. Zhong, X.L. Zou, C. Bourdelle, S.D. Song, J.F. Artaud, T. Aniel, X.R. Duan, Convective Velocity Reversal Caused by Turbulence Transition in Tokamak Plasma, Phys. Rev. Lett. **111**, 265001(2013)

[16] M.N. Rosenbluth, M.L. Sloan, Finite-β Stabilization of the Collisionless Trapped Particle Instability, Phys. Fluids **14**, 1725(1971)

[17] J.W. Connor, R.J. Hastie, T.J. Martin, Effect of pressure gradients on the bounce-averaged particle drifts in a tokamak, Nucl. Fusion **23**, 1702(1983)

[18] B.B. Kadomtsev, O.P. Pogutse, *Reviews of Plasma Physics Vol. 5*, (Consultants Bureau, NY, 1970): Also Sov. Phys. JETP **24**, 1172(1967)

[19] G. Rewoldt, W.M. Tang, M.S. Chance, Electromagnetic kinetic toroidal eigenmodes for general magnetohydrodynamic equilibria, Phys. Fluids **25**, 480(1982)

[20] A. Pochelon, T.P. Goodman, M. Henderson, et al., Energy confinement and MHD activety in shaped TCV plasmas with localized electron cyclotron heating, Nucl. Fusion **39**, 1807(1999)

[21] Y. Camenen, A. Pochelon, R. Behn, A. Bottino, A. Bortolon, S. Coda, A. Karpushov, O. Sauter, G. Zhuang and the TCV team, Impact of plasma triangularity and collisionality on electron heat transport in TCV L-mode plasmas, Nucl. Fusion **47**, 510 (2007)

[22] M. Fontana, L. Porte, S. Coda, O. Sauter and TCV Team, The effect of triangularity on fluctuations in a tokamak plasma, Nucl. Fusion **58**, 024002(2018)

[23] M. Fontana, (2018) Turbulence studies in TCV using the Correlation ECE diagnostic, EPFL PhD thesis No 9016 (https://infoscience.epfl.ch/record/258091/files/EPFL_TH9016.pdf)

[24] O. Sauter, S. Brunner, D. Kim, G. Merlo, R. Behn, Y. Camenen, S. Coda, B.P. Duval, L. Federspiel, T.P. Goodman, A. Karpushov, A. Merle, and TCV Team, On the non-stiffness of edge transport in L-mode tokamak plasmas, Phys. Plasmas **21**, 055906(2014)

[25] G. Merlo, S. Brunner, O. Sauter, Y. Camenen, T. Gorler, F. Jenko, A. Marinoni, D. Told, L. Villard, Investigating profile stiffness and critical gradients in shaped TCV discharges using local gyrokinetic simulations of turbulent transport, Plasma Phys. Control. Fusion **57**, 054010(2015)

[26] F. Riva, E. Lanti, S. Jolliet, P. Ricci, Plasma shaping effects on tokamak scrape-off layer turbulence, Plasma Phys. Control. Fusion **99**, 035001(2017)

[27] M. Austin, A. Marinoni, M.L. Walker, et al., High confinement in negative triangularity discharges in DIII-D, 59th APS-DPP Bulletin Bo4 2 (2017)

[28] A. Marinoni, H-mode-like confinement with L-mode edge in negative triangularity plasmas on DIII-D, Abstract MF-I54 in 1st Asia-Pacific Conference on Plasma Physics, 18-23 September, 2017, Chengdu, China. http://aappsdpp.org/DPPP2017rogramlatest/pdf/MF-I54.pdf

[29] M. Austin, A. Marioni, et al., High Confinement in Negative Triangularity Discharges in DIII-D, 27th IAEA Fusion Energy Conference, 22-27 October 2018, Ahmedabad, India, https://nucleus.iaea.org/sites/fusionportal/Shared%20Documents/FEC%202018/FEC2018_ConfMat_Online.pdf, paper EX/P6-6

[30] A. Marinoni, et al., APS-DPP 2018 Invited talk, to be submitted to Physics of Plasmas.

[31] H. Nakamura, et al., H-mode experiments with outer and lower divertors in JT-60, Nuclear Fusion **30**(1990)235

[32] T. Ohkawa, V.S. Chan, M.S. Chu, R.R. Dominguez, R.L. Miller, New Current Drive and Confinement Techniques for Improved Tokamak Operation, In Plasma Physics and Controlled Nuclear Fusion Research (Proc. 12th Int. Conf. Nice, 1988), IAEA, Vienna (1989), Vol. 1, p. 681

[33] M.D. Kruskal, C.R. Oberman, On the Stability of Plasma in Static Equilibrium, Phys. Fluids **1**, 275(1958)

[34] F. Porcelli, M.N. Rosenbluth, Modified Mercier criterion, Plasma Phys. Control. Fusion **40**, 481(1998)

[35] A. Merle, O. Sauter, S. Yu Medvedev, Pedestal properties of H-modes with negative triangularity using the EPED-CH model, Plasma Phys. Control. Fusion 59, 104001(2017)

[36] A. Loarte and G. Federici, private communication.

[37] Y. Takahashi, T. Isono, K. Hamada, et al., Technology development and mass production of Nb_3Sn conductors for ITER toroidal field coils in Japan, Nucl. Fusion **51**, 113015 (2011)

[38] L. Bottura, B. Bordini, $J_c(B,T,\varepsilon)$ Parametrization for the ITER Nb_3Sn Production, IEEE Trans. Appl. Supercond., **19**(2009)1521

[39] J-M Rey, A. Allais, J-L Duchateay, et al., Critical current measurement in HTS *Bi2212* ribbons and round wires, IEEE Trans. Appl. Superconduct., **19**(2009)3088

[40] T. Ando, H. Nakajima, H. Hiue, and Y. Wadayama., The Effect of Ti conduit on the critical current in $(N_bT_i)_3S_n$ cable-in-donduit conductors, IEEE Transactions on Applied Superconductivity Vol. 3, pp. 488-491 (1993)

[41] N. Cheverev, et al., ITER TF conductor insert manufacturing, IEEE Trans. Appl. Superconductivity, vol. 12, pp. 548-553 (2002)

[42] N. Martovetsky, et al., Test of the ITER TF insert and Central Solenoid Model Coil, IEEE Trans. Appl. Superconductivity, vol. 13, pp. 1441-1446 (2003)

[43] S. Nishio, K. Tobita, S. Konishi, T. Ando, et al., Tight aspect ratio tokamak power reactor with superconducting TF coils, IAEA-CN-FT/P1-21, in 19th IAEA Fusion Energy Conference (Lyon, France, Oct. 2002)

[44] T. Ando, S. Nishio, Design of high T_c superconducting TF coil for the tight aspect ratio tokamak power plant, IEEE Trans. Appl. Superconduct., vol 14, 1481(2004)

[45] T. Ando, S. Nishio, Design of the TF coil for a tokamak fusion power reactor with YBCO tape superconductors, Fusion Technology (2006)

[46] J. Jiang et al. (MagLab), August 2017 unpublished (National magnetic field laboratory homepage:https://nationalmaglab.org/magnet-development/applied-superconductivity-center/plots)

[47] O. Sauter, Geometric formulas for system codes including the effect of negative triangularity, Fusion Engineering and Design **112**, 633(2016)

[48] D. Chen, J. Jiang, Y. Hou, W. Duan, M. Ni, C. Xing, Preliminary Cost Assessment and Compare of China Fusion Engineering Test Reactor, J. Fusion Energy (2015) 34:127-132. DOI 10.1007/s10894-014-9770-x

[49] T. Takizuka, S. Tokunaga, K. Hoshino, K. Shimizu, N. Asakura, Combination of helical ferritic-steel inserts and flux-tube expansion divertor for the heat control in tokamak DEMO reactor, J. Nucl. Materials **463**, 1229(2015)

[50] A. Herrmann, Overview on stationary and transient divertor heat loads, Plasma Phys. Control. Fusion *44*, 883(2002)

[51] H. Zohm, C. Angioni, E. Fable, G. Federici, et al., On the physics guidelines for a tokamak DEMO, Nucl. Fusion **53**, 073019(2013)

[52] L. Villard, et al., Global turbulence features across marginality and nonlocal pedestal-core interactions, Plasma Phys. Contr. Fusion, to be published.

[53] E.J. Doyle, W.A. Houlberg, et al., Progress in the ITER Physics Basis Chapter 2, Plasma confinement and transport, Nucl. Fusion **47**, S18(2007)

[54] S. Sengoku, A. Funahashi, et al., Regime of Improved Confinement in Neutral-Beam-Heated Limiter Discharges of a Tokamak, Phys. Rev. Lett. **59**, 450 (1987)

[55] S. Tsuji, K. Ushigusa, et al., Observation of the Limiter H-mode in the JT-60 Tokamak with Lower-Hybrid Current Drive, Phys. Rev. Lett. **64**, 1023 (1990)

[56] K. Toi, K. Kawahata, et al., Role of Edge Magnetic Shear on the Limiter H-mode Transition of the JIPP T-IIU Tokamak, Phys. Rev. Lett. **64**, 1895 (1990)

[57] J. Moret, M. Anton, et al., Ohmic H-mode and confinement in TCV, Plasma Phys. Contr. Fusion **37**, A215(1995)

[58] M. Kikuchi, M. Azumi, Frontier in Fusion Research II – Introduction to Modern Tokamak Physics, Springer (2015)

[59] The National Academy of Sciences, Final Report of the Committee on a Strategic Plan for U.S. Burning Plasma Research, December 13, 2018. https://www.nap.edu/catalog/25331/final-report-of-the-committee-on-a-strategic-plan-for-us-burning-plasma-research

[60] K. Hoshino, N. Asakura, K. Shimizu, et al., Divertor Study on DEMO Reactor, Plasma and Fusion Research, **9**, 3403070 (2014)

[61] ITER Physics Basis Editors, ITER Physics Expert Group Chairs and Co-Chairs, ITER JCT and Physics Integration Unit, ITER Physics Basis, Chapter 1: Overview and summary, Appendix A , Nucl. Fusion 39, 2137 (1999).

[62] ITER Physics Expert Groups on Confinement & Transport and Confinement Modelling & Database and ITER Physics Basis Editors, ITER Physics Basis, Chapter 2: Plasma confinement and transport, Nucl. Fusion **39**, 2175 (1999).

Table 1 Major coil parameters of three TF coil designs in Figure 5

	A=3, R_p=9m	A=3, R_p=7m	A=3.5, R_p=7m
Coil shape	Racetrack	Racetrack	Racetrack
Coil size	15m x 20m	12m x 16m	11m x 14m
Number of coils	18	18	18
Magnetic Energy	170GJ	86.5GJ	104GJ
Maximum field	13.6T	13.5T	15.5T
Ampere Turn	263MAT	207MAT	263MAT
Discharge constant	12 s	10 s	12 s
Quench detection	2 s	2 s	2 s
Temperature rise	150K	150K	150K
Number of Turn/coil	116	116	146
Conductor current	126kA	100kA	100kA
Winding structure	ITER-like	ITER-like	ITER-like
Disk per coils	6	6	7
Terminal voltage	12.5kV	10kV	10kV

Table 2 TF conductor designs of three reactor configurations in Figure 5 (*A=3, R_p=9m; A=3, R_p=7m; A=3.5 R_p=7*m)

	A=3, R_p=9m		A=3, R_p=7m		A=3.5, R_p=7m	
Conductor type	Nb3Sn CIC(SS)	Nb3Sn CIC (Ti)	Nb3Sn CIC(SS)	Nb3Sn CIC (Ti)	Nb3Sn CIC	Bi2212
Operating current	126kA	126kA	100kA	100kA	100kA	100kA
Nominal field	13.6T	13.6T	13.5T	13.5T	15.5T	15.5T
Operating Temperature	5.0K	5.0K	5.0K	5.0K	5.0K	20K
Total operating strain	-0.6%	-0.05%	-0.6%	-0.05%	-0.05%	0.2%
Current sharing Temp.	6.1K	6.2K	6.1K	6.1K	6.2K	21.2K
Operating curr./Crit. curr.	0.64	0.56	0.61	0.56	0.72	0.89
Cable diameter	62.0mm	57.8mm	56.0mm	50.8mm	54.0mm	54.6mm
Central cooling (ID/OD)	11mm/ 9mm	11mm/ 9mm	11mm/ 9mm	11mm/ 9mm	11mm/ 9mm	11mm/ 9mm
Central coolant	Supercritical He	Supercritical He	Supercritical He	Supercritical He	Supercritical He	Gas He
Conductor outer diameter	66.0mm	61.8mm	60.0mm	54.8mm	58.0mm	58.6mm
Jacket material	SS	Ti	SS	Ti	Ti	No jacket
SC and Cu strand diameter	0.84mm	0.87mm	0.84mm	0.76mm	0.81mm	0.82mm
Cu/Non Cu, Ag/ non Ag	1.0	2.0	1.0	2.0	1.6	0.82
Cabling pattern	3x3x4x4x4x6	3x3x3x4x4x6	3x3x3x4x4x6	3x3x3x4x4x6	3x3x3x4x4x6	3x3x3x4x4x6
SC strand number	2304	1440	1728	1728	1728	864
Cu, Ag strand number	1152	1152	864	864	864	1728
Void fraction(%) in bundle	33.3%	33.3%	33.3%	33.3%	33.3%	0%
Impregnated material	No impregnation	No impregnation	No impregnation	No impregnation	No impregnation	PbSn

Table 3 Steady-state operation parameters from the system code corresponding to three cases in Figure 5. Temperature and density profiles are assumed as $T(r)=T_0(1-(r/a)^2)1.3$, $n(r)=n_0[0.9(1-(r/a)^2)]^{0.5}+0.1]$.

No	Input Parameter	Symbol	A=3, R_p=9m	A=3, R_p=7m	A=3.5, R_p=7m
1	Plasma current (MA)	I_p	21	15.4	13.2
2	Toroidal field (T)	B_t	5.86	5.94	7.53
3	Major radius (m)	R_p	9.0	7.0	7.0
4	Aspect Ratio	A	3.0	3.0	3.5
5	Elongation at separatrix	κ_x	2.0	2.0	1.85
6	Upper and lower triangularity at sep.	δ_u / δ_l	-0.4 / -0.9	-0.4/-0.9	-0.4/-0.9
7	Normalized beta	β_N	2.1	2.7	2.5
8	Greenwald fraction	f_{GW}	0.85	0.85	0.85
9	Confinement enhancement over y2 scaling	H_H	1.12	1.5	1.5
10	Helium fraction	f_{He}	0.05	0.05	0.05
11	Impurity fraction	f_{imp}	0.002	0.0019	0.002
12	Current drive efficiency (10^{20}A/W/m^2)	η_{CD}	0.5	0.5	0.5
No	Output parameters	Symbol	A=3, R_p=9m	A=3, R_p=7m	A=3.5, R_p=7m
1	Minor radius (m)	a_p	3.0	2.333	2.0
2	Cylindrical safety factor	q_{cy}	3.49	3.75	3.60
3	Bootstrap current fraction	f_{bs}	0.30	0.41	0.39
4	Effective Charge	Z_{eff}	1.73	1.67	1.71
5	Line average density (α_n=0.5) (10^{20}m^{-3})	$\bar{n}_e$	0.63	0.77	0.89
6	Volume av. temperature (α_T=1.3) (keV)	$\langle T_e \rangle$, $\langle T_i \rangle$	16.9	17.1	17.2
7	Plasma volume (m^3)	V_p	3235	1522	1025
8	Plasma surface (m^2)	S_p	1789	1082	870
9	Fusion power (MW)	P_F	2964	2053	1862
10	Neutron flux (MW/m^2)	Γ_n	1.33	1.52	1.71
11	Total heating power (MW)	P_{tot}	761	507	473
12	Current drive power (MW)	P_{CD}	168	96.6	101
13	Transport loss power (MW)	P_{transp}	594	384	338
14	Radiation loss power (MW)	P_{rad}	167	124	135
15	Energy gain	Q	17.7	21.3	18.5
16	Energy confinement time (s)	τ_E	2.80	2.51	2.24
17	Poloidal beta	β_p	1.08	1.50	1.57
18	Toroidal beta (%)	β_t	2.51	3.0	2.19

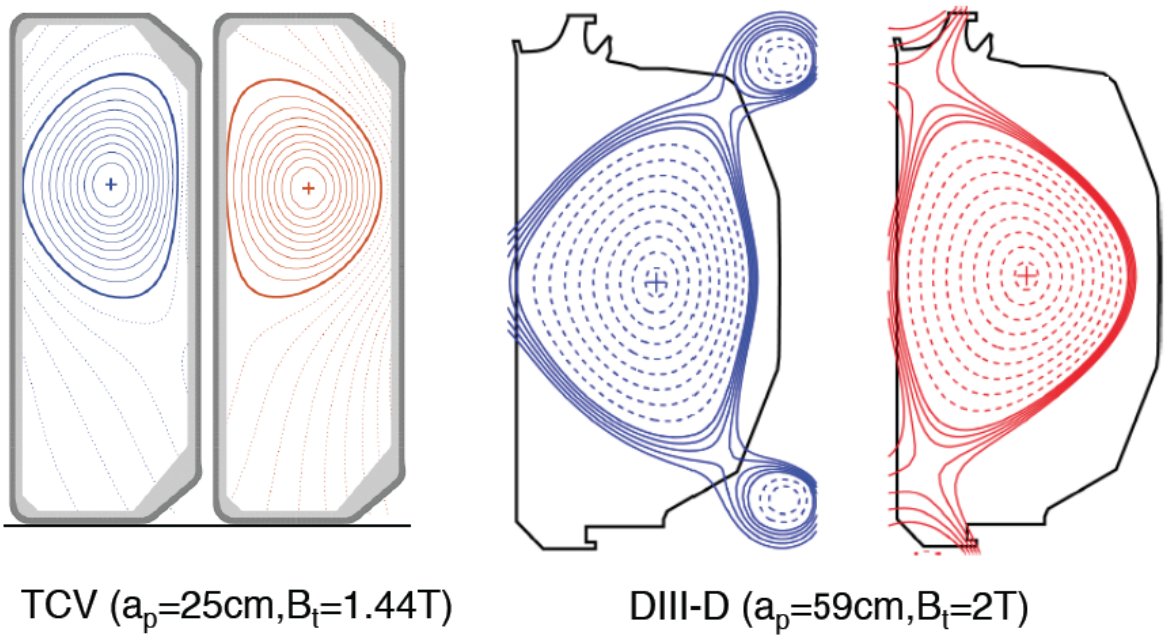

Figure 1 D-shaped and NTT experimental configurations in TCV (PT:$S=9.9m^2$, NT:$10.3m^2$) and DIII-D (PT:$S=42m^2$, NT:$S=45m^2$). Here S is plasma surface area.

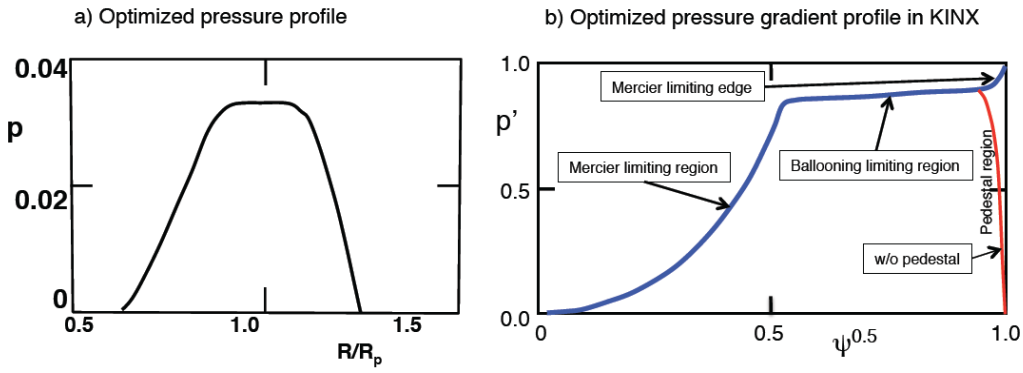

Figure 2 a) Optimized pressure profile in NTT. Near-flat profile near the plasma center. b) Mercier limiting region and ballooning limiting region. Comparison of Mercier limiting edge and zero gradient edge.

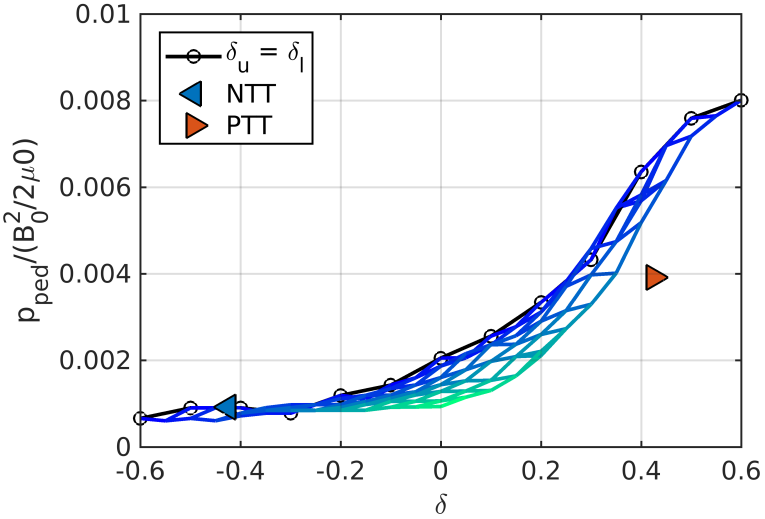

Figure 3 Normalized pedestal pressure limit determined by EPED-CH code as a function of average triangularity δ. Parameters used are R_p=9m, a_p=3m, B_t=5T, I_p=15MA, κ_x=1.8, δ_l=-0.85, δ_u=0 for the NTT and δ_l=+0.85, δ_u=0 for the standard D-shaped plasma [30]. The color indicates deviation from up–down symmetry going from blue to green for more asymmetry(color online).

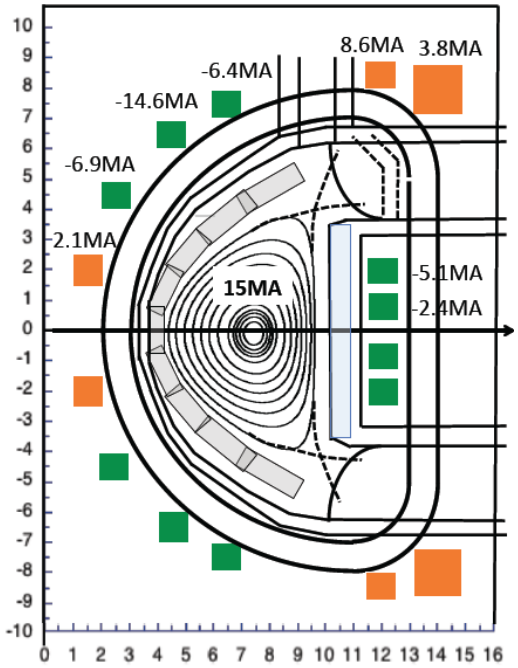

Figure 4 Inverted D-shaped Toroidal Field Coil for original κ_x=1.5 DN-NTT configuration (R_p=7m, a_p=2.7m, δ=-0.9, I_p=15MA, B_t=6.2T.

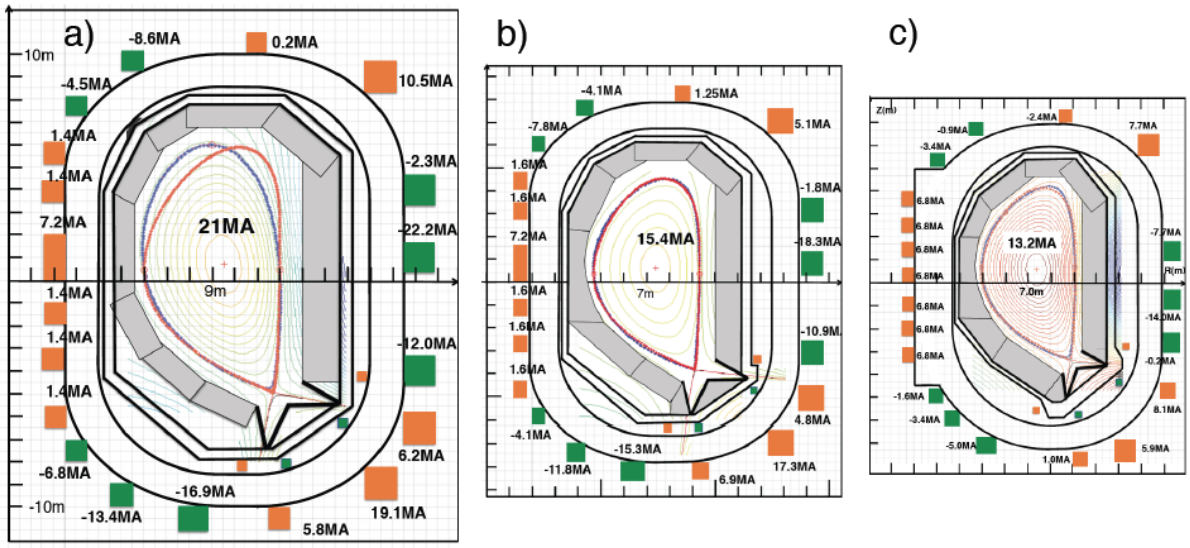

Figure 5 Configuration designs of NTT reactors. Here, green-colored PF coils are for pushing and orange-colored PF coils are for attracting (color online).

a) *A=3* conservative design (I_p=21MA, B_t=5.86T, B_{max}=13.6T, R_p=9m, δ_u=-0.4, δ_l=-0.9, κ_x=1.8, l_i=0.84, β_N=2.1) [10],

b) *A=3* high confinement (I_p=15.4MA, B_t=5.94T, B_{max}=13.5T, R_p=7m, δ_u=-0.4, δ_l=-0.9, κ_x=2.0, H_H=1.50, l_i=0.85, β_N=2.7, β_N^{NW}=2.89),

c) *A=3.5* high field and high confinement (R_p=7m, δ_u=-0.4, δ_l=-0.9, κ_x=1.85, H_H=1.5, B_t=7.53T, B_{max}=15.5T, l_i=0.91, β_N=2.5, β_N^{NW}=2.87).

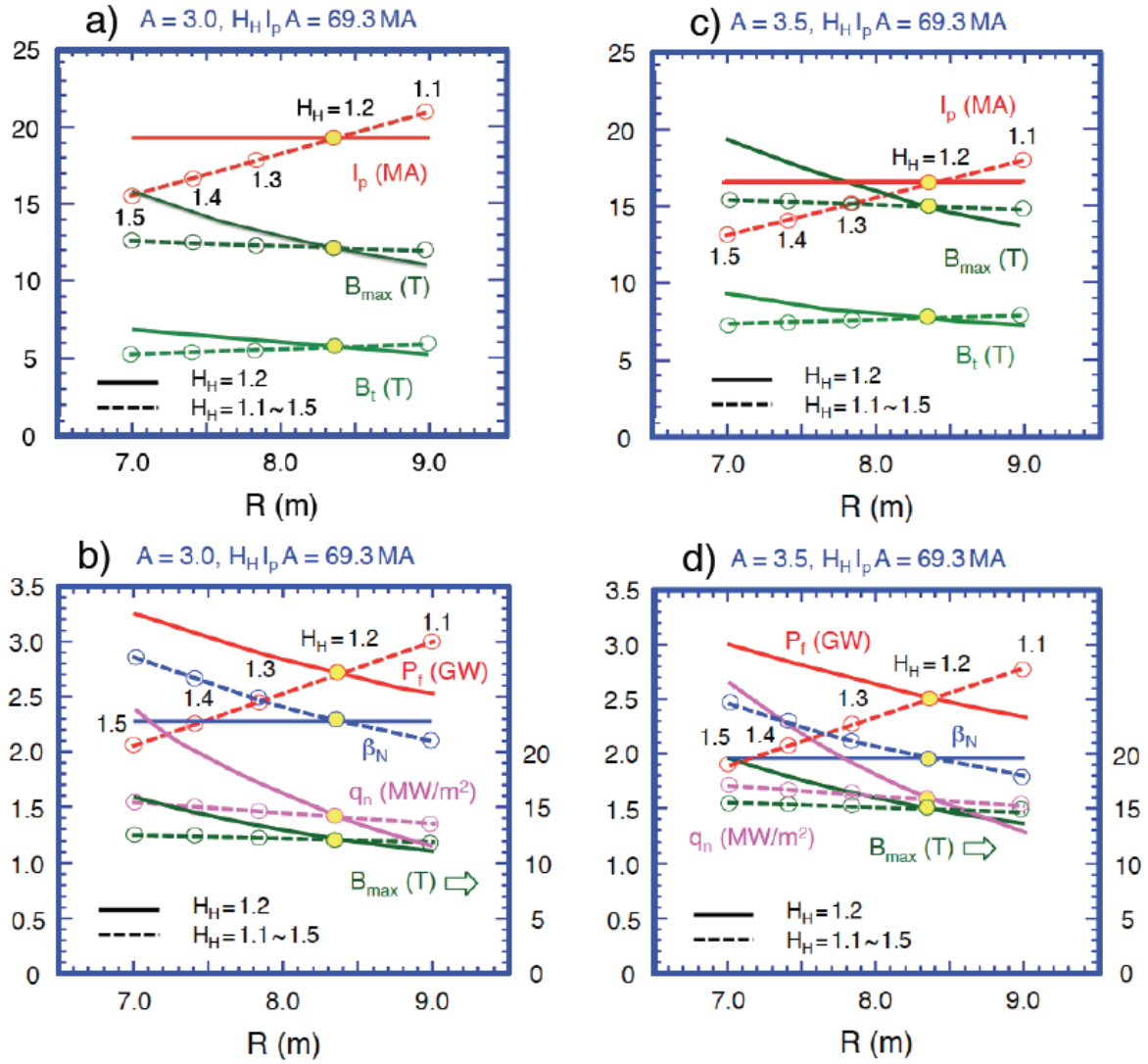

Figure 6 Parameter surveys of NTT reactor designs. a) R_p scan of I_p, B_{max}, B_t for fixed H_H=*1.2* (solid line) and H_H=*1.1-1.5* (broken line) (A=*3*), b) R_p scan of P_f, β_N, q_n for fixed H_H=*1.2*(solid line) and H_H=*1.1-1.5* (broken line) (A=3), c): R_p scan of I_p, B_{max}, B_t for fixed H_H=*1.2*(solid) and H_H=*1.1-1.5* (broken)(A=*3.5*), d) R_p scan of P_f, β_N, q_n for fixed H_H=*1.2* (solid line) and H_H=*1.1-1.5* (broken line) (A=*3.5*).

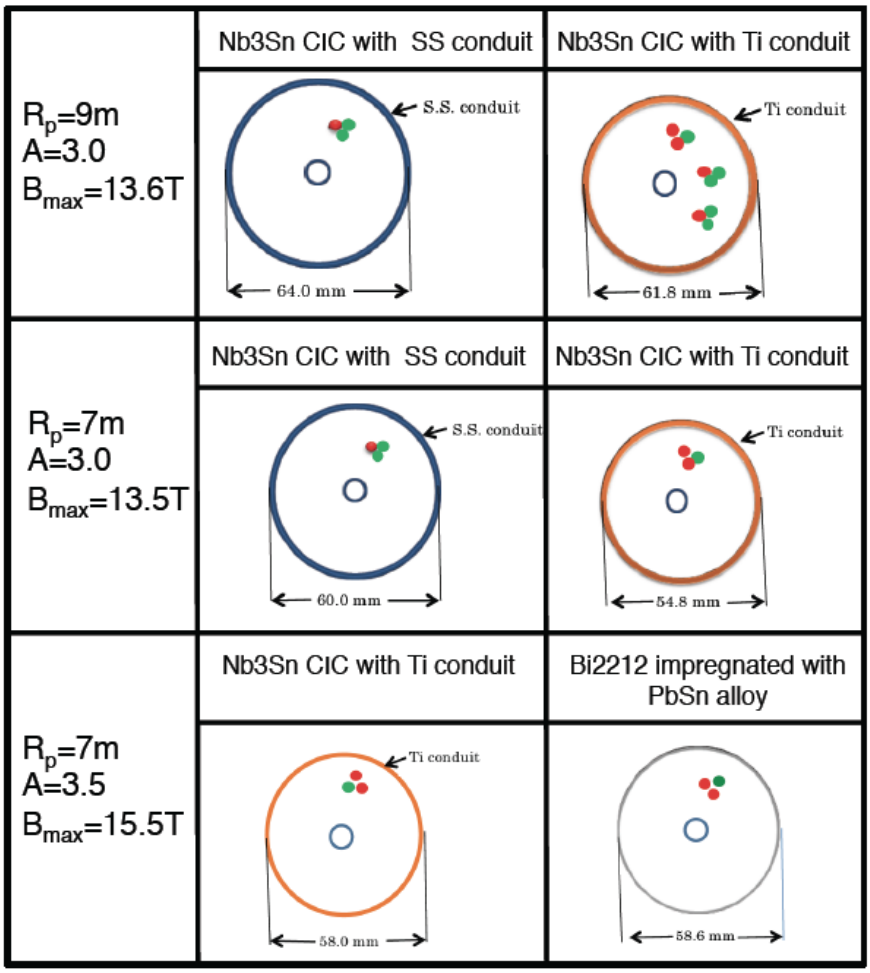

Figure 7 Conductor designs of three reactor configurations. The blue circle is *SS* conduit and the orange circle is T_i conduit. Green closed circle is superconducting strand and the red closed circle is *Cu* strand for low temperature SC and *Ag* strand for high T_c SC (*Bi2212*) (color online).

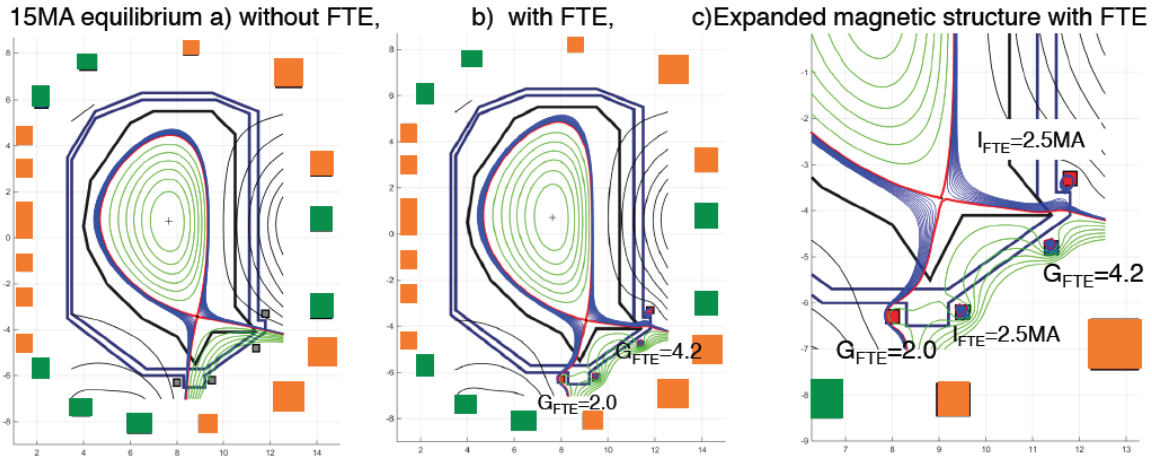

Figure 8 Divertor geometry of *Ip=15MA, Rp=7m* equilibrium without FTE and with FTE coil current (I_{FTE}*=2.5MA*) . Flux tube expansion by 2.0 and 4.2 are obtained for inner and outer divertor legs, respectively.

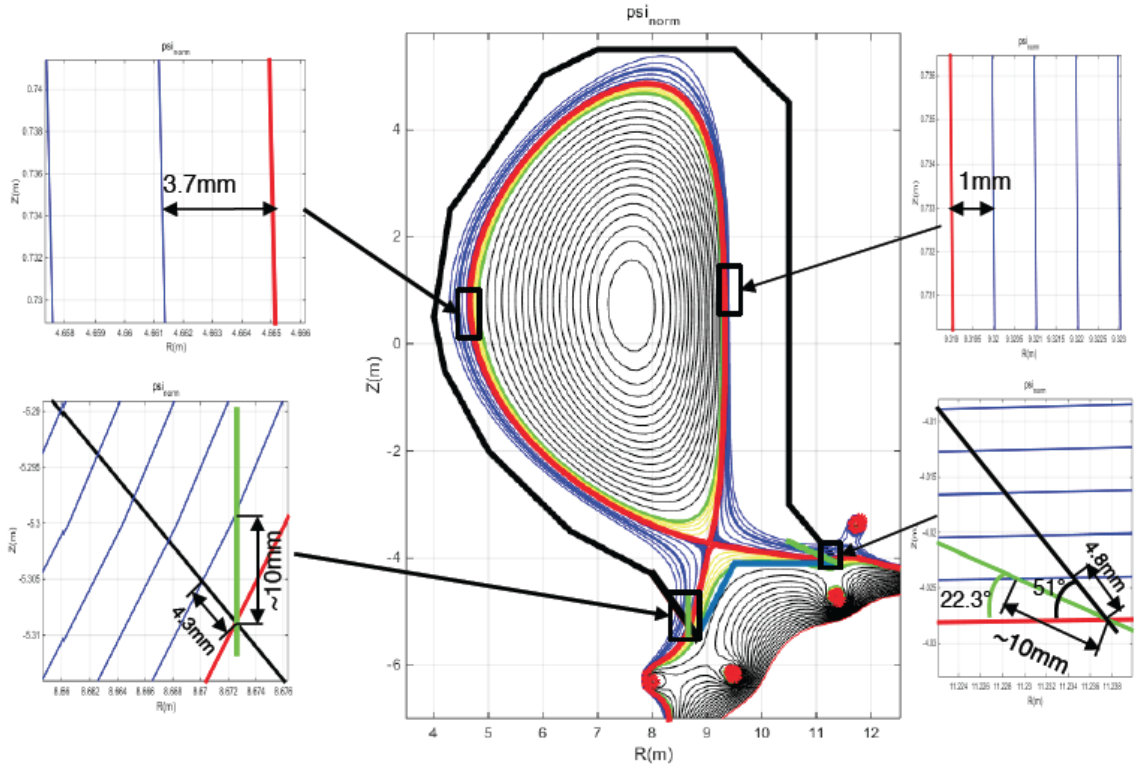

Figure 9 Divertor geometries for NTT (I_p=*15MA,* R_p=*7m,* I_{FTE}=*2.5MA*). For a 1mm SOL width at outboard mid-plane, inboard mid-plane thickness is *3.7mm*. Use of FTE coils expanded the flux tube and *4-5 mm* along the divertor plate for the original semi-open divertor target geometry (black lines). With more inclined divertor targets, 1mm SOL at outboard mid-plane will be projected to *10mm* along the divertor plates (green lines) (color online).

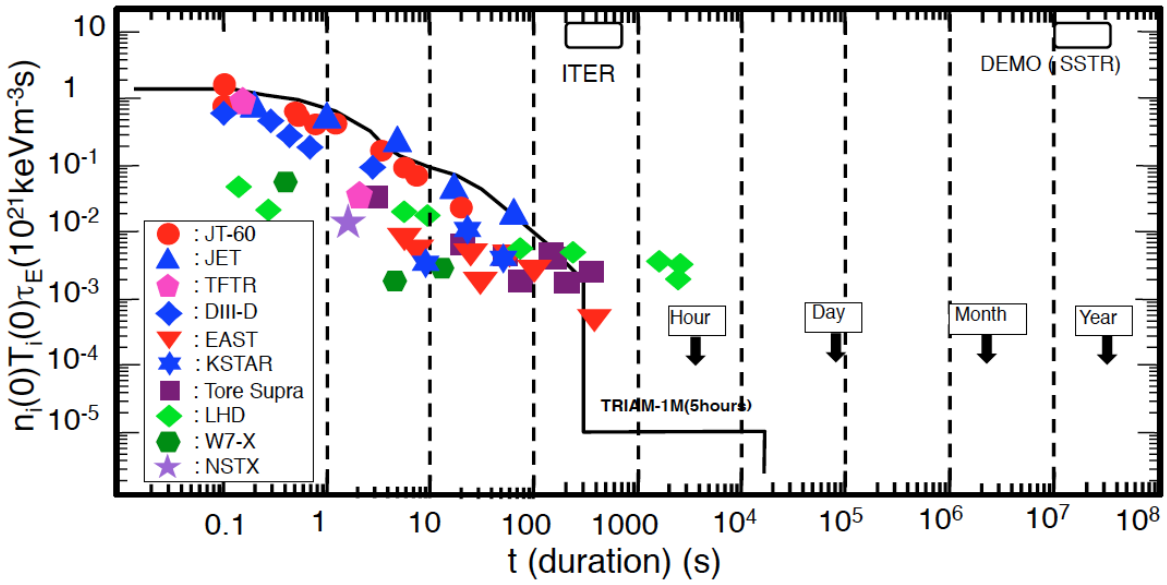

Figure 10 Achieved fusion triple product ($n_i(0)T_i(0)\tau_E$) as a function of sustained duration [53]. Data points are added for the US NAS report contributed from B. Wan, H. Park, T. Pedersen, P. Snyder, S. Kaye [54].